1990A&A...230..200A

Astron. Astrophys. 230, 200–212 (1990)

ASTRONOMY AND ASTROPHYSICS

Physical parameters of solar Hα absorption features derived with the cloud model

C.E. Alissandrakis[1], G. Tsiropoula[2], and P. Mein[3]

[1] Section of Astrophysics, Astronomy and Mechanics, Department of Physics, University of Athens, Panepistimiopolis, GR-15783 Athens, Greece
[2] Astronomical Institute, National Observatory of Athens, P.O. Box 20048, GR-11810 Athens, Greece
[3] Observatoire de Paris Meudon, Section Astrophysique, F-92195 Meudon Principal Cedex, France

Received April 27, accepted August 20, 1989

Abstract. We present observations of a fibril region and of an arch filament region obtained by the Multichannel Subtractive Double Pass Spectrograph (MSDP) operating in Hα at the Pic du Midi Observatory. Intensity fluctuations and Doppler shift velocities were derived over two dimensional fields of view. The observed contrast profiles have been matched with theoretical contrast profiles based on the cloud model which has four parameters: the line-of-sight velocity, the source function, the optical depth and the Doppler width. We have taken into account the fact that the cloud model is valid only in a restricted range of circumstances. Contour maps and histograms of the 4 parameters were made for these regions and a comparison of the velocities given by 3 different methods (cloud model, Doppler shift and the "3-optical depths" method of Mein and Mein, 1988) is made.

Key words: lines: profile – Sun: chromosphere – Sun: activity

1. Introduction

One of the fundamental problems in the analysis of disturbed line profiles is the determination of the physical quantities which are related to that part of the atmosphere where the line is formed. In particular, the detection of velocity fields in the solar atmosphere is a problem of continuous interest, since a large amount of observational data shows evidence of substantial mass motions in many solar features. The analysis of these velocity fields is an essential step in understanding the mechanisms of bulk plasma acceleration and energy transfer.

Various methods have been used in the past in order to derive physical parameters from the observed profiles. It is a common practice to measure Doppler velocities by determining the wavelength of a point midway between two positions of equal intensity in the absorption line profile. Here the moving structure is naively assumed to produce its own line profile, which is simply shifted with respect to the background profile by an amount $\Delta\lambda_I = \lambda_0 v/c$, where v is the line-of-sight velocity. The determination of the velocities in this way sometimes yields inconsistent results due to the lack of knowledge of the effective height of formation of the lines considered (Kulander and Jefferies, 1966; Beckers, 1968; Athay, 1970).

The "cloud" model suggested by Beckers (1964) has also been used extensively for the description of chromospheric absorption features seen in the Balmer lines. However, the parameters yielded by this model, e.g. velocity, source function, optical depth and Doppler width, have no physical meaning if this model is used without caution. Good agreement with theoretical NLTE calculations are obtained in the case of high altitude loops (Cram, 1986). However, it is obvious that this model cannot be applied to low lying structures which are not sufficiently separated from the chromospheric background. Recently, two kinds of "differential cloud" models have been proposed (Mein and Mein, 1988) called "cloud models of order one and two" which take into account a realistic background profile; in addition a procedure for the determination of the 4 cloud model parameters has been developed by the same authors. This procedure will be called "3-optical depths" method in the following sections (see Sect. 5.3 for the description of the method).

The purpose of this work is to use carefully the cloud model for processing large quantities of spectral data in two-dimensional fields of view and to compare the results of this model to those of the dopplershift method and the "3-optical depths" method.

2. Application of Beckers' cloud model

The contrast profile technique introduced by Beckers (1964) has been used extensively in the analysis of observations of identifiable fine structures (Grossmann-Doerth and von Uexküll, 1971, 1973, 1977), Bray (1973, 1974), Bray and Loughhead (1983). According to this empirical approach every structural element of the chromosphere is assumed to consist of a "cloud" lying between the observer and a stationary reference atmosphere, whose line profile is known. The model provides a quantitative description of the spatial variations of the physical parameters which are responsible for the observed inhomogeneities. It is fully described by 4 parameters: the function

$$S = \int_0^{t_v} S_v \exp(-\tau_v) d\tau_v \Big/ \int_0^{t_v} \exp(-\tau_v) d\tau_v$$

Send offprint requests to: G. Tsiropoula

© European Southern Observatory • Provided by the NASA Astrophysics Data System

1990A&A...230..200A

which is identical to the source function if the latter is frequency-independent; the optical depth at line center, τ_0; the line broadening parameter, $\Delta\lambda_D$, which yields the kinetic temperature and microturbulence; the Doppler shift of the line absorption coefficient, $\Delta\lambda_I$, which yields the line-of-sight component of the mass velocity.

The intensity is expressed in terms of the "undisturbed background" in order to give a quantity that can be related conveniently to observations, namely the contrast. Assuming that the source function is frequency-independent and moreover that it is constant throughout the cloud, the contrast of a structural element is given by the expression:

$$C(\Delta\lambda)=\frac{I(\Delta\lambda)-I_0(\Delta\lambda)}{I_0(\Delta\lambda)}$$

$$=\left(\frac{S}{I_0(\Delta\lambda)}-1\right)(1-\exp(-\tau(\Delta\lambda))) \quad (1)$$

where $I_0(\Delta\lambda)$ is the reference profile emitted by the background atmospheric layer. In addition one assumes that the wavelength dependence of the optical thickness is gaussian:

$$\tau(\Delta\lambda)=\tau_0\exp\left(-\left(\frac{\Delta\lambda-\Delta\lambda_I}{\Delta\lambda_D}\right)^2\right) \quad (2)$$

and that $\Delta\lambda_I$ and $\Delta\lambda_D$ are constant throughout the cloud.

Refering to Eq. (1), we note that the second term in the right-hand side is always positive and decreases with $\Delta\lambda$. Thus, it is the first factor of this equation that determines the sign of the contrast (bright or dark feature). For the chromospheric Hα reference profile which increases with $\Delta\lambda$, this factor decreases with $\Delta\lambda$. We can thus distinguish three classes of contrast profiles predicted by the cloud model, according to the ratio of the source function to the background intensity:

1. If $I_0(\Delta\lambda)>S$ the first factor in Eq. (1) is negative throughout the profile and the model predicts a dark feature at all wavelengths.

2. If $I_0(\Delta\lambda=0)<S$, then $S=I_0(\Delta\lambda_1)=I_0(\Delta\lambda_2)$, where $\Delta\lambda_1$ is a wavelength displacement greater than 0 and $\Delta\lambda_2$ is less than 0; in this case the first factor of Eq. (1) is positive near the line center but its sign reverses at $\Delta\lambda_1$ and $\Delta\lambda_2$ and becomes negative in the wings. The model predicts a cloud bright at line center but dark in the wings.

3. If $I_0(\Delta\lambda)<S$, which means that the intensity of the background profile is smaller than the source function at all wavelengths, the first factor of Eq. (1) becomes positive and the model predicts a bright cloud at all wavelengths.

Grossmann-Doerth and von Uexküll (1971) as well as Bray (1973) applied this model to chromospheric mottles observed at disk centre and derived values for the 4 parameters from all the observed contrast profiles. However, this model failed to explain contrast profiles near the limb (Loughhead, 1973) or some contrast profiles of sunspot fibrils (Bray, 1974). In this later paper Bray argued that the cloud model cannot be applied to all the observed profiles. The height of the structure relative to the region over which the Hα line is formed plays a decisive role in shaping the observed profile. Thus, only profiles of features lying at such a height that the Hα line is entirely formed before their lower boundary, can be matched by this model. This view was confirmed by theoretical analyses carried out by Durrant (1975). On the other hand only under the assumption that the mass velocity, the Doppler width and the source function are constant along the line-of-sight is this model applicable.

3. Observations

Observations in the Hα chromosphere reveal many types of dark filamentary structures which are strong indicators of the magnetic field orientation. Among them systems of arch-shaped filaments are an essential part of developing active regions. They occur in the interspot region of bipolar sunspot groups, they bridge the neutral line and connect regions of opposite magnetic polarities. Their appearance is accompanied by an enhancement of the magnetic field which grows and expands into the corona. Thus they are believed to be the optical manifestation of magnetic flux tubes emerging from the subphotospheric layers. Bruzek (1967) called them arch-filament systems (AFS) and from an analysis of Hα filtergrams he found that the material moves along them following the direction of the magnetic field. In a later analysis of Hα filtergrams and Hα spectra, Bruzek (1969) showed that material flows downward in both branches of the arch, while the top ascends. This latter picture is generally accepted for the motion of the AFS until today.

A striking aspect of isolated sunspots when seen in Hα photographs is a well-ordered pattern of elongated dark structures called "fibrils". Fibrils constitute the basic structures of the outer superpenumbra and stream in a direction of opposite polarity. Knowledge of their flow velocity is a useful probe in understanding the chromospheric Evershed effect. Both these structures, e.g. AFS and fibrils, are located at such a high level (>4000 km), that one can assume safely that the Hα line is formed below the lower boundary of the structure. Thus these structures are ideal for the application of the cloud model.

The present observations were made with the Multichannel Double Pass spectrograph (MSDP) mounted on the 50 cm "Tourelle" refractor of the Pic du Midi Observatory. This instrument records a two dimensional field on the solar surface with 1″×1″ spatial resolution (Mein, 1977). The observations of the AFS region (Active Region 4819 with coordinates N20 E20) were made on June 22, 1987 at $7^h25^m22^s$UT (Fig. 1) simultaneously in 10 wavelengths, 0.256 Å apart in the Hα profile. The observations of the fibrils were made on October 19, 1983 at $9^h06^m41^s$ UT (Fig. 2) in Active Region 4340. The coordinates of this region were S10 W25. Observations were made simultaneously in 9 wavelengths, with the same spacing between the channels as above. From these observations line profiles have been reconstructed using the standard reduction methods for this type of data. Maps of intensity and Doppler velocities have been computed from the profiles by a code simulating a "lambdameter" technique at $\Delta\lambda=\pm0.3$ Å and $\Delta\lambda=\pm0.6$ Å (Mein, 1977). Two regions have been selected and studied: the first contains 3 fibrils with 100×126 (=12 600) structural elements covering a field of view of 22″×28″ (pixel size 0″.222); the second contains 3 arch filaments with 100×121 (=12 100) structural elements covering a field of view of 25″×30″ (pixel size 0″.250).

4. Data reduction

As background profile in our computations we have taken the one given by the atlas spectrum. A line profile which emanates from the interior of the supergranular cells has been measured and published by Grossmann-Doerth and von Uexküll (1973),

© European Southern Observatory • Provided by the NASA Astrophysics Data System

1990A&A...230..200A

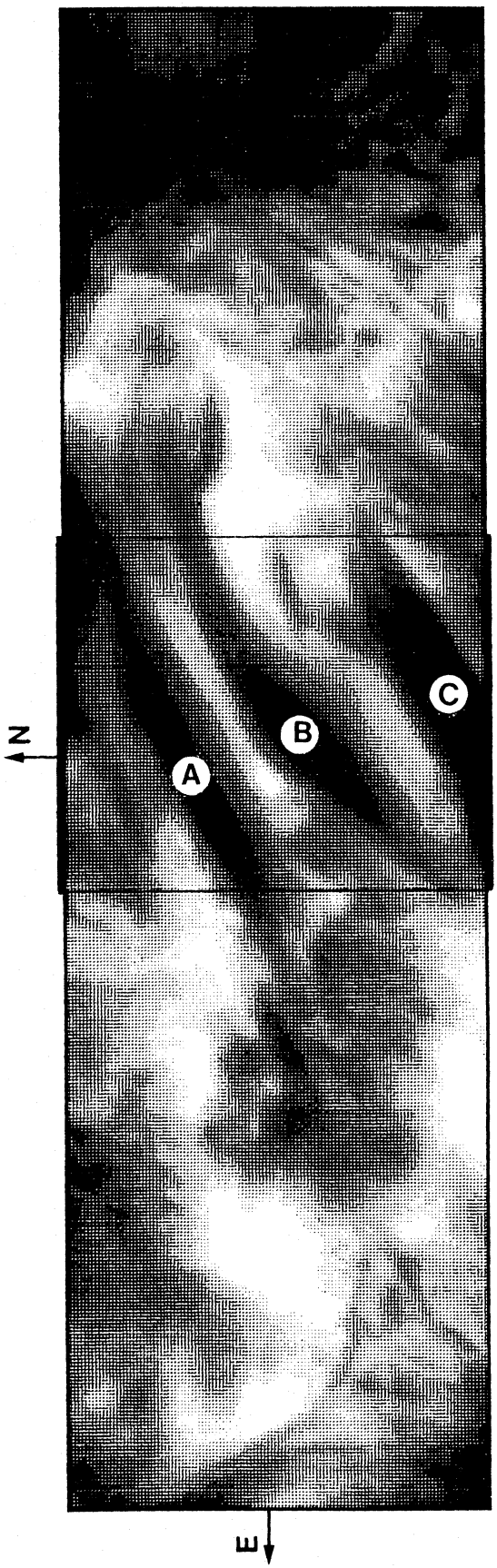

Fig. 1. Computed intensity map at the center of Hα of an active region at N20 E20 observed from the Pic du Midi with the MSDP on June 22, 1987, at 7:25:22 UT. The rectangle containing the arch filament region studied in this paper is drawn

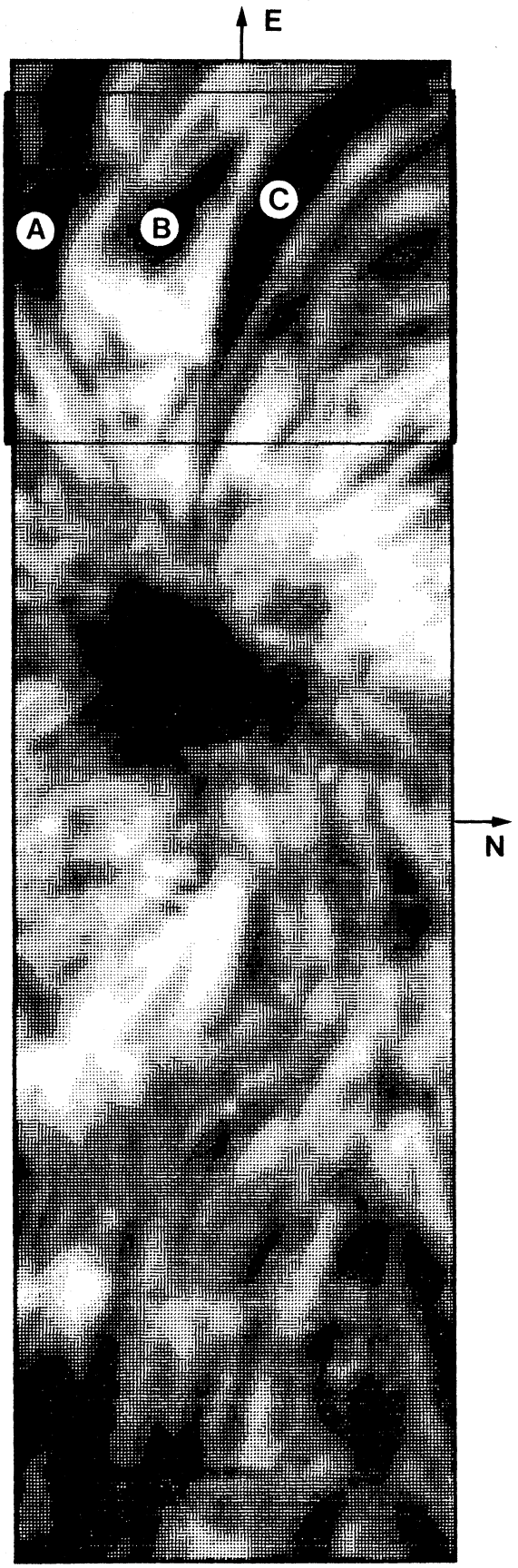

Fig. 2. Computed intensity map at the center of Hα of an active region at S10 W25 containing superpenumbral fibrils, observed from the Pic du Midi with the MSDP on October 19, 1983 at 9:06:41 UT. The rectangle containing the fibril region studied in this paper is drawn

© European Southern Observatory • Provided by the NASA Astrophysics Data System

1990A&A...230..200A

but we consider that the use of this profile would not change qualitatively our results.

The atlas profile is actually the average profile, integrated over all fine structures; thus the question of whether this could be considered as the background profile, in the sense required by the cloud model, is raised. As every observer knows, the appearance of filtergrams obtained at the line center is very different from those obtained in the wings of Hα. In the wings one observes distinct absorption features overlaid above a more or less uniform background, while at the center of the line the fine structures are so closely packed that it is doubtful whether we can see any emission which comes from the lower part of the chromosphere. Therefore, the atlas profile is a much better approximation to the background profile in the wings than at the line center. For this reason we have ignored the central channel of MSDP data; so 8 channels instead of 9 have been used in the case of the fibrils and 9 instead of 10 in the case of the arch filaments. Thus our cloud computation starts at roughly 0.26 Å from the line center.

Considerable caution must be exercised in applying the cloud model to the interpretation of contrast observations. So, it is obvious that the following types of contrast profiles should be rejected:

1. Profiles that are bright throughout (or nearly). Clearly this is not the case for the dark features under study.

2. Profiles that are bright near the line center and dark in the wings. According to Durrant (1975) profiles of this type correspond to "low" clouds, which act back on the radiation field underneath and thus violate the crucial condition of the cloud model. For this type of profile Beckers' model fails to provide meaningful information for the 4 physical parameters.

3. Profiles for which the values of contrast at equal wavelength displacements $\pm\Delta\lambda$ on either side of the Hα center do not have the same sign (Bray, 1974). From Eq. (1) we obtain:

$$\frac{C(+\Delta\lambda)}{C(-\Delta\lambda)} = \frac{1-\exp(-\tau(+\Delta\lambda))}{1-\exp(-\tau(-\Delta\lambda))} \tag{3}$$

which shows that the right-hand side is always positive and the same must be true for the left. Profiles that do not have this property cannot be interpreted in terms of the cloud model.

These 3 restrictions above, can be combined in the following one: all profiles that have a maximum value of contrast less than 0.1 have been processed; we have taken a maximum value of 0.1 instead of zero in order to consider also profiles that have positive values because of instrumental noise and also in order to take into account the fact that the background profile is not well known near the line center.

The computation of the 4 parameters was carried out by an iterative least-square procedure for non-linear functions which was repeated until the ratio between two consecutive χ^2 values was smaller than 1.005. Hα contrast profiles that are negative nearly throughout [which correspond to clouds sufficiently high to be detached from the standard atmosphere (Durrant's model B)] have been fitted by this procedure. In high clouds it was confirmed that Beckers' cloud model gives correct values for the 4 parameters (Durrant, 1975).

The initial values for the iteration procedure were taken in the following way: for the source function, which primarily determines the value of the contrast at line center we used the approximate expressions:

$S = 175 + 220\, C(\Delta\lambda = 0)$ in the case of the AFS and

$S = 155 + 159\, C(\Delta\lambda = 0)$ in the case of the fibrils;

which were found empirically from some good fits (here and in the rest of the paper the source function is given in units of 1/1000 of the continuum intensity); for the optical depth at line center we used an initial value of 1; for the Doppler width we used 0.5 Å in the case of the AFS and 0.3 Å in the case of the fibrils; finally for the Doppler shift parameter we used a value of −0.1 Å if the minimum of the contrast was at the violet side and 0.1 Å if it was at the red side.

After the fitting procedure, we rejected:

1. Values of S that were greater than 200. The intensity of the atlas profile at the line center is about 170, but we have some profiles bright at line center because of the selection rule concerning the maximum value of the contrast. Obviously, profiles with S greater than 170 may not be accurately treated with the cloud model, as discussed above.

2. Values of τ_0 that are greater than 5. By stipulating that the optical depth be small we ensure that the structures under study cannot build up their own radiation.

Computations were also performed by using all the MSDP channels; the results were not very different except at the edges of the structures where more profiles could be considered when the central channel was rejected.

The least square fit code computes the uncertainties of the fit for each parameter, which gives the change of the particular parameter that doubles the rms of the residuals. The influence of the background profile on the velocity values will be discussed in the next section.

Table 1. Cloud parameters for the AFS region

Parameters	Average value	Standard deviation	Average uncertainty
Velocity (in km s^{-1})	−3.4	6.5	1.9
Source function	152.0	14.0	9.3
Optical depth	1.30	0.34	0.38
Doppler width (in Å)	0.54	0.11	0.06

5. Results and discussion

5.1. Arch filaments

Approximately 2200 structural elements satisfying the criteria discussed in the previous section were treated in the AFS region. The results are shown in the form of contour maps in Fig. 3, while Table 1 gives the average value and standard deviation of each parameter and the average uncertainties of the fit.

Figure 3a shows the source function; it has a smooth variation with a minimum value of 130 to 140 near the center of each filament. Near the edge of the filaments the source function exceeds the value of the background intensity at the line center (which is equal to 170). This happens primarily because we accepted contrast profiles which were slightly bright in order to account for the noise and also because we ignored the central channel of the MSDP. In any case, the results of such regions should be treated with some caution; therefore only pixels with source function less than 170 were used for the histograms and the scatter plots in this paper. Comparing Fig. 3a with Fig. 1 one has

© European Southern Observatory • Provided by the NASA Astrophysics Data System

1990A&A...230..200A

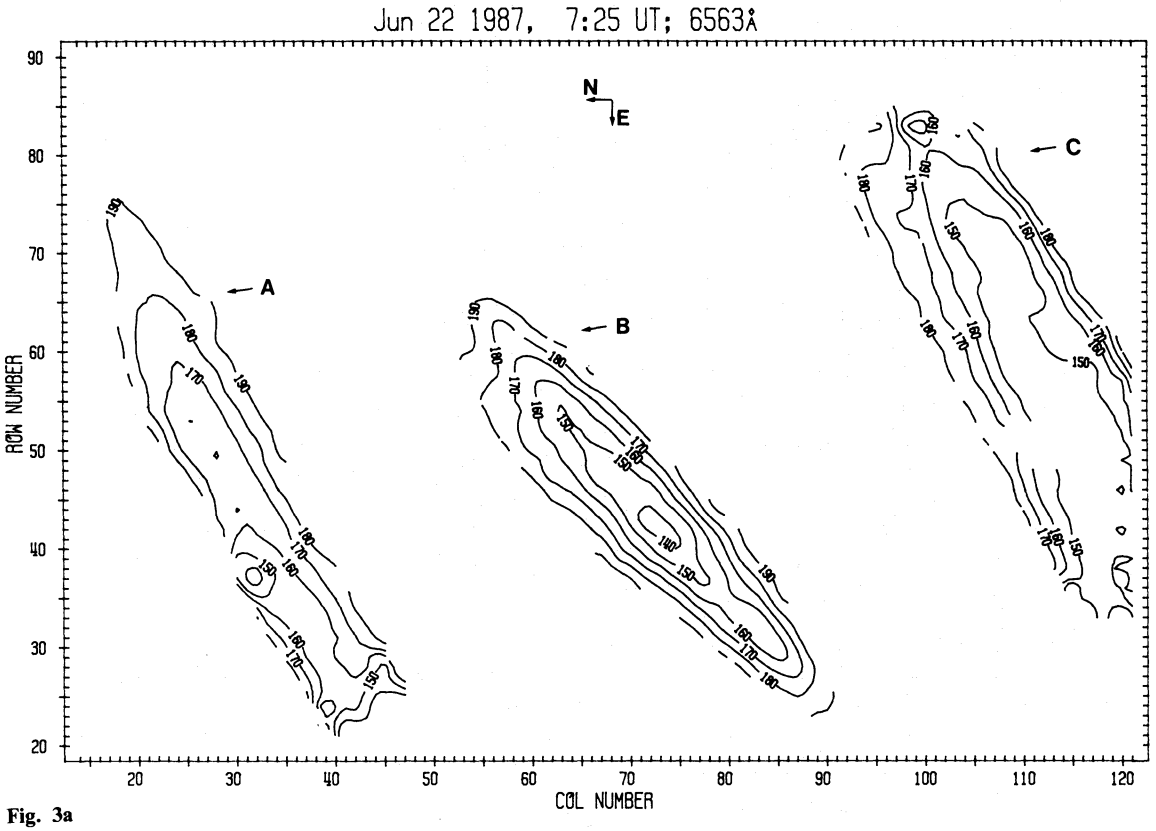

Fig. 3a

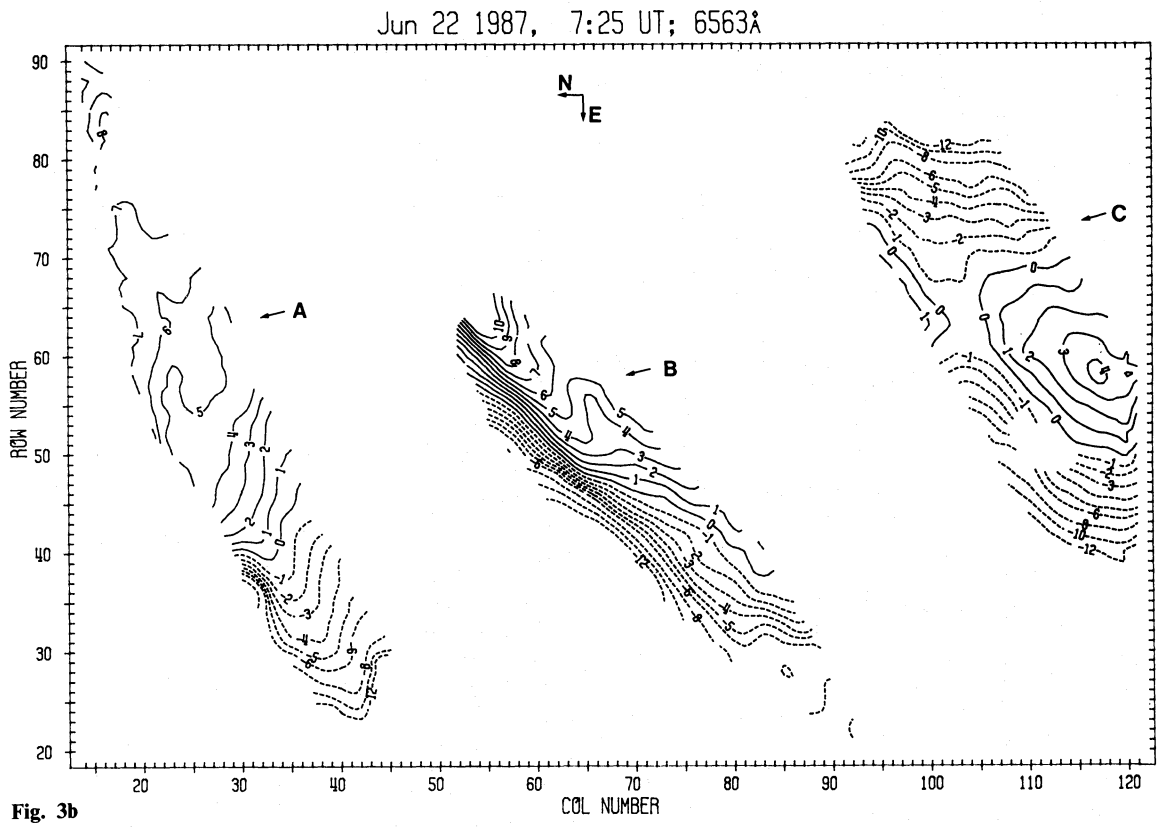

Fig. 3b

Fig. 3a–d. Contour maps of the 4 parameters derived with the cloud model in the AFS region (for A, B, C see text): **a** source function; **b** velocity (full lines refer to velocities towards the observer dashed lines to velocities of opposite direction); **c** Doppler width; **d** optical depth

© European Southern Observatory • Provided by the NASA Astrophysics Data System

1990A&A...230..200A

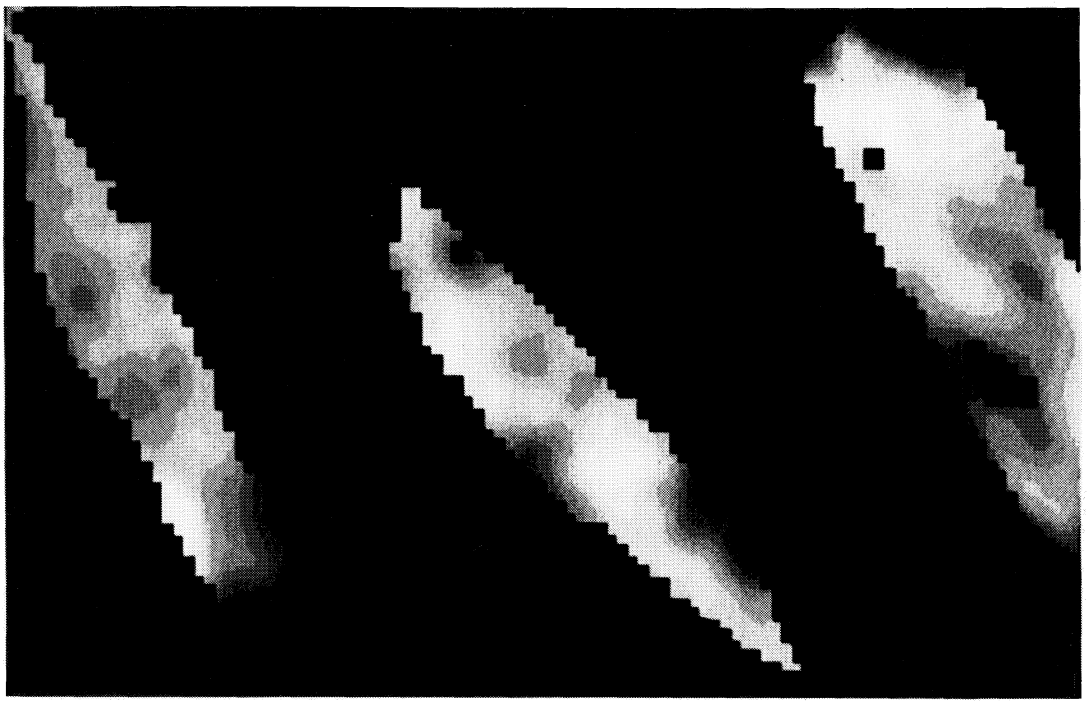

Fig. 3c

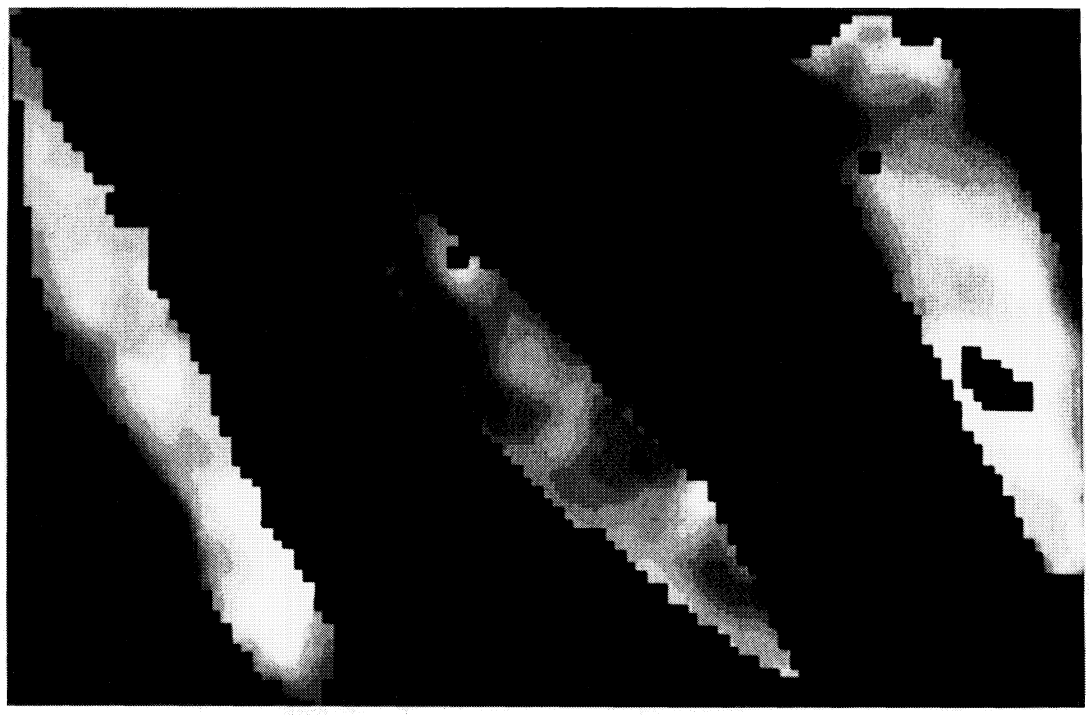

Fig. 3d

the impression that the actual arch filaments are more extended than the regions selected by our code; this apparently means that only the central part of the filament satisfies the condition of "high cloud" discussed in the previous section. The histogram of the source function peaks around 155 with values as low as 60 (Fig. 4a).

Figure 3b shows the map of the line-of-sight velocity. The velocity structure of the filament C has the typical form, with material moving towards the observer (i.e. ascending) near the top of the filament with a line-of-sight velocity of up to 4 km s^{-1} and away from the observer near the feet of the filament with a line-of-sight velocity larger than 10 km s^{-1}. The situation is different in

© European Southern Observatory • Provided by the NASA Astrophysics Data System

1990A&A...230..200A

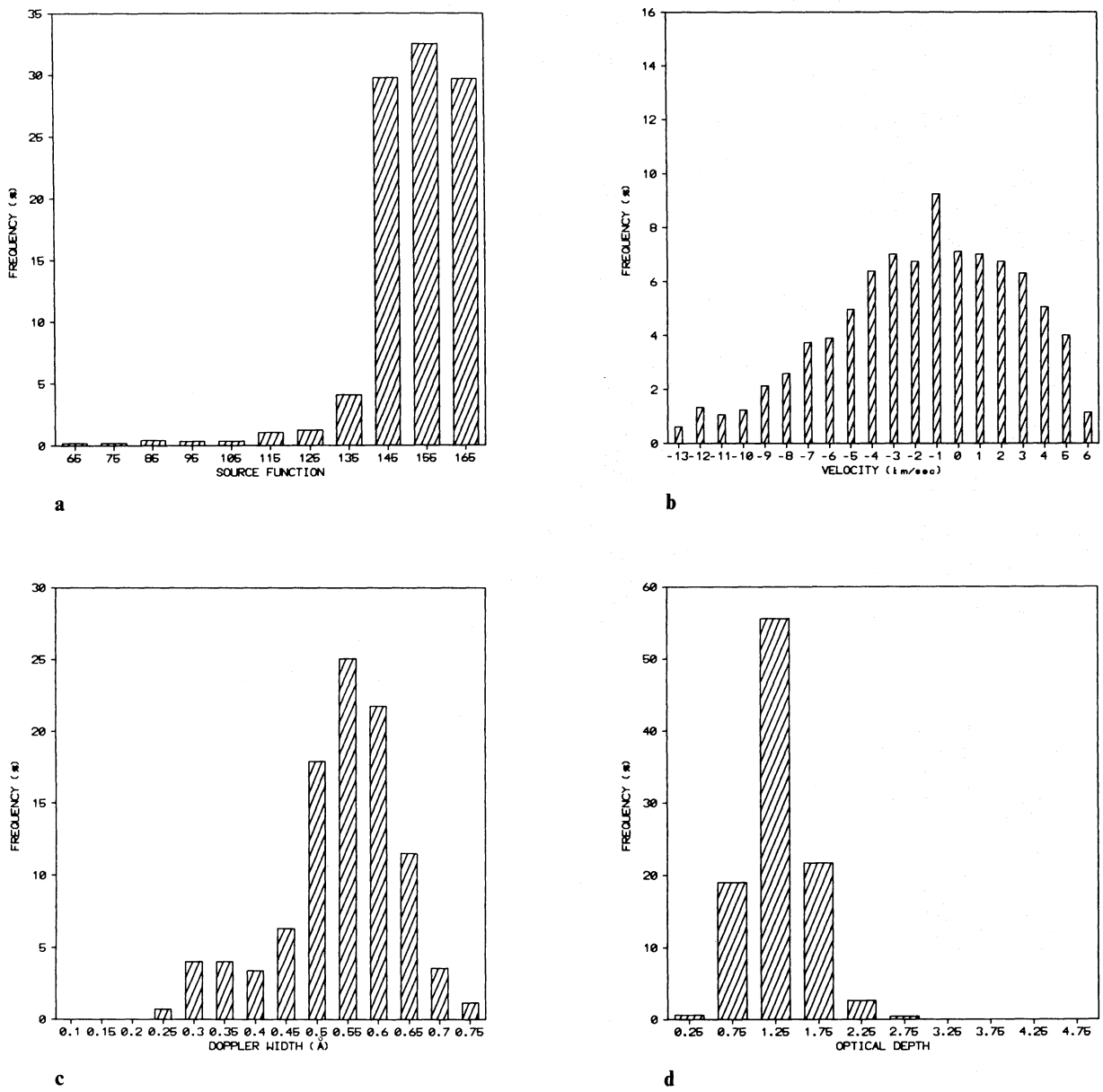

Fig. 4a–d. Histograms of the 4 parameters derived with the cloud model in the AFS region: **a** source function; **b** velocity; **c** Doppler width; **d** optical depth

the other two filaments; in filament A the line-of-sight velocity is negative only near its east feet (up to 10 km s^{-1}) while in filament B the zero velocity contour is almost parallel to the filament axis. We should, however, keep in mind that our maps do not show the entire filament. The velocity histogram (Fig. 4b) peaks around -1 km s^{-1}, with individual values ranging from about -20 km s^{-1} to 8 km s^{-1}; it is asymmetric, with more pixels having negative velocity than positive. We note that the isothermal sound velocity for a hydrogen gas at 15 000 K is about 11 km s^{-1}.

Figures 3c and 3d show maps of the Doppler width and the optical depth at line center. We note that regions of high Doppler width have low optical depth. This is not surprising since the absorption coefficient at line center is:

$$\alpha_\lambda = \frac{\sqrt{\pi}e^2}{mc^2}\frac{f\lambda^2}{\Delta\lambda_D}\varphi(\lambda) \tag{4}$$

where $\varphi(\lambda)$ is the profile of the absorption coefficient, with $\varphi(\lambda_0)=1$ and f the oscillator strength. Thus the optical depth at line center is:

$$\tau_0 = N_2 L \alpha_0 \approx N_2 L/\Delta\lambda_D \tag{5}$$

where N_2 is the number density in the second hydrogen level and L is the geometrical thickness of the structure. The anticorrelation between τ_0 and $\Delta\lambda_D$ implies that the quantity $N_2 L$ varies little over the arch-filaments. Using Eq. (5) and the mean values of τ_0 and $\Delta\lambda_D$ (Table 1) we can estimate a mean value for

© European Southern Observatory • Provided by the NASA Astrophysics Data System

1990A&A...230..200A

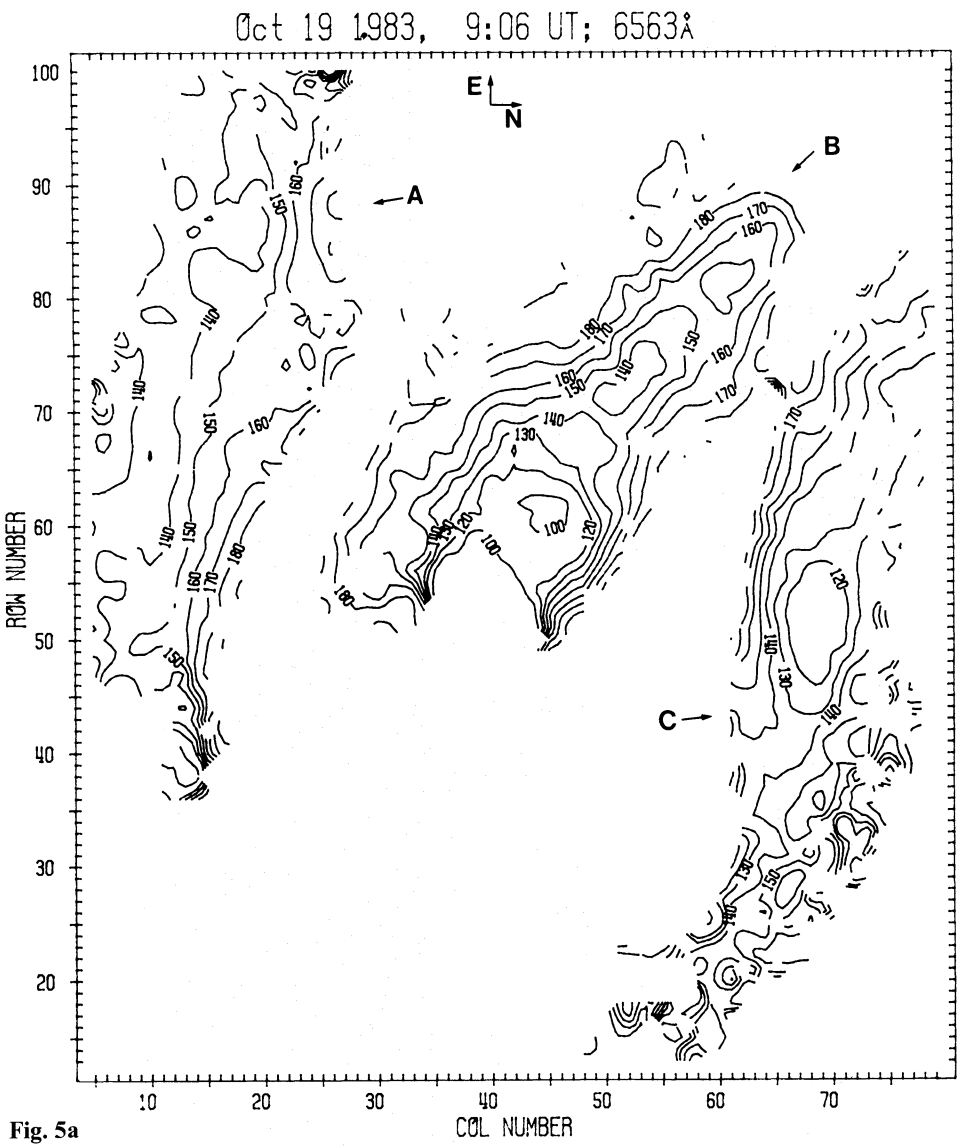

Fig. 5a

Fig. 5a–d. Contour maps of the 4 parameters derived with the cloud model in the fibril region (for A, B, C see text): **a** source function; **b** velocity; **c** Doppler width; **d** optical depth

the quantity N_2L; this is equal to $5.2\,10^{12}\,\mathrm{cm}^{-2}$. L being 1.7–2.7 10^8 cm, N_2 takes values in the range 2–3 $10^4\,\mathrm{cm}^{-3}$.

Both maps show smooth variations with no apparent relation of either quantity with the source function or the velocity structure. The Doppler width peaks around 0.55 Å, with values ranging from about 0.25 Å to 0.75 Å (Fig. 4c). We note that according to Vernazza et al. (1973), the chromospheric temperature is about 6500° K, which corresponds to a thermal Doppler width of 0.23 Å. The microturbulence in a Doppler width of 0.55 Å and if the temperature is 6500° K is about $22.8\,\mathrm{km\,s}^{-1}$, while if the temperature is 15000° K it takes the value of $19.4\,\mathrm{km\,s}^{-1}$. Thus the microturbulence seems to be an important contributor. The histogram of optical depth peaks around 1.25, with individual values ranging from 0.1–3.0 (Fig. 4d) suggesting that, at least, the studied structural elements are not optically very thick.

5.2. *Superpenumbral fibrils*

Approximately 3200 structural elements satisfying the criteria discussed in the previous section were treated in the fibril region of Fig. 2. The maps of the cloud parameters are given in Fig. 5, the respective histograms in Fig. 6, while Table 2 gives the average value, standard deviation and average uncertainty of the fit for each parameter.

Figure 5a shows the map of the source function. Here again the variation from the centre to the edge of each fibril is smooth with a minimum of 120 to 130 for fibrils *A* and *C* and 90 for fibril *B*. The histogram of the source function (Fig. 6a) peaks around 145 with values as low as 60.

Figure 5b shows the map of the line-of-sight velocity, which is predominantly negative. This fibril region is located near the principal spot of the active region; the spot is outside the region shown in Fig. 5b and at the lower side (see also Fig. 2). It is interesting to consider whether the velocity field is associated with the Evershed flow which, at the chromospheric level, manifests itself as a material motion towards the spot. Due to projection effects the line-of-sight velocity is expected to be negative at the diskward side of the spot and positive at the limbward side (e.g. Dialetis et al., 1985). Indeed, our region is located at the diskward side, hence the predominance of negative line-of-sight velocity. We note further an overall decrease of the velocity (in absolute

© European Southern Observatory • Provided by the NASA Astrophysics Data System

1990A&A...230..200A

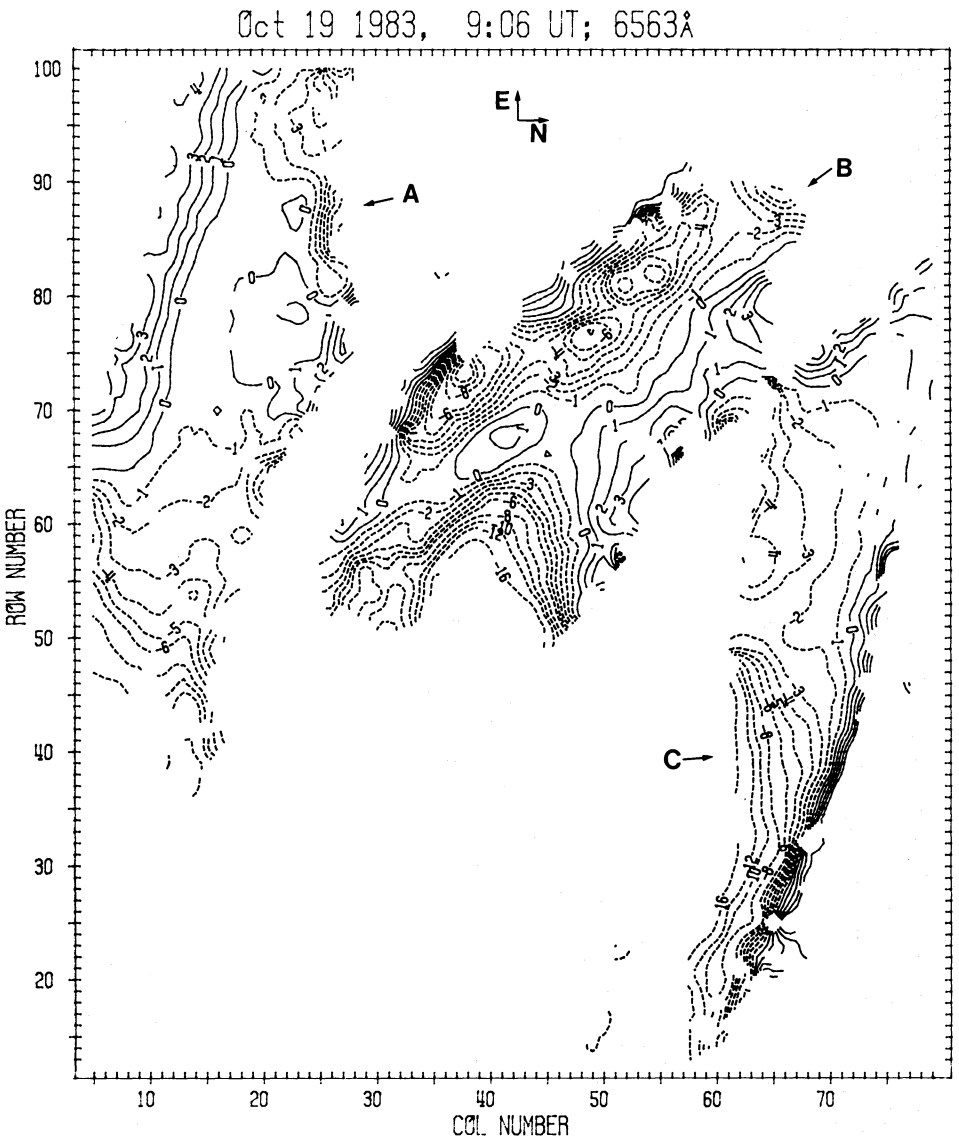

Fig. 5b

values) with distance from the spot, which is expected to occur in the outward region of the Evershed flow (Alissandrakis et al., 1988). The histogram of the line-of-sight velocity (Fig. 6b) peaks around $0\,\mathrm{km\,s^{-1}}$ with individual values of $-22\,\mathrm{km\,s^{-1}}$ to $12\,\mathrm{km\,s^{-1}}$.

Figures 5c and 5d show maps of the Doppler width and the optical depth at line center. We note again the anticorrelation between these two quantities as in the case of the AFS. Using the average values of τ_0 and $\Delta\lambda_D$ given at Table 2 we can estimate from Eq. (5) the average value of the quantity $N_2 L$; this is equal to $3.7\,10^{12}\,\mathrm{cm^{-2}}$. L being between 2.8–$3.7\,10^8$ cm, N_2 takes values between 0.7–$1.3\,10^4\,\mathrm{cm^{-3}}$. The Doppler width peaks around 0.25 Å with values ranging from 0.1 Å to 0.75 Å (Fig. 6c). The optical depth peaks around 1.25 with individual values ranging from 0.05 to 4.5 (Fig. 6d). Fibril A has systematically smaller values of Doppler width and greater values of optical depth than the other two.

Comparing the distributions of the parameters in these two different kinds of features we notice the following: on the average, the value of the source function is smaller in the fibrils than in the arch filaments; in both cases we have optically thin structures with about the same average value of the optical depth; the average value of the Doppler width is lower in the fibrils implying that the temperature and/or the microturbulence velocity are lower in these structures.

Many authors have pointed out that the source function and the Doppler width should depend on each other (Durrant, 1975; Cram, 1986; Steinitz et al., 1977). However, no such relation was found from our results; moreover no correlation between any of the parameters in our two samples was found except the anticorrelation between τ_0 and $\Delta\lambda_D$ mentioned above.

A linear interpolation of the source function as a function of the contrast at line center gives: $S = 178.0 + 217.4\,C(\Delta\lambda = 0)$ in the case of the AFS and $S = 156.0 + 177.3\,C(\Delta\lambda = 0)$ in the case of the

© European Southern Observatory • Provided by the NASA Astrophysics Data System

1990A&A...230..200A

Fig. 5c

Fig. 5d

Table 2. Cloud parameters for the fibril region

Parameters	Average value	Standard deviation	Average uncertainty
Velocity (in km s^{-1})	−2.3	6.3	2.5
Source function	141.0	23.0	16.0
Optical depth	1.55	1.12	1.57
Doppler width (in Å)	0.32	0.12	0.08

fibrils, relations that are not very different from those used for estimating the initial values of the source function in the fitting procedure.

Quite frequently estimates of the velocity of chromospheric features are made, based on the wavelength where the particular feature shows up most prominently in series of filtergrams along the Hα profile. In order to test this method we examined the correlation between the wavelength where the contrast is minimum (maximum in absolute value) and the velocity derived from the cloud model. No correlation was found, which implies that naive interpretations of line asymmetries can lead to grossly inaccurate estimates of the velocity (cf. Beckers, 1964, who first pointed out this fact).

5.3. Relation between the velocities given by the 3 different methods

A contour map of the velocity given by the Doppler shift method at ±0.3 Å is shown in Fig. 7 for the AFS region. As can be seen there is no indication of the features or their boundaries in this velocity map. On the other hand, doppler shift measurements provide too small velocity values. A comparison between the velocities given by the cloud model and the Doppler velocities (at ±0.3 Å) is shown in Fig. 8 for the same region. Cloud velocities are about 2 to 5 times greater than Doppler velocities. We must notice, however, that the general behavior is exactly the same, e.g. positive or negative velocities given from the two methods are found at the same places; the fibril region shows the same behavior.

A comparison between the velocities obtained with the present method and the method proposed by Mein and Mein (1988), (the "3-optical depths" method) is shown in Fig. 9 for the AFS region. According to this method the source function S is taken to be between 0 and $I_0(\Delta\lambda=0)$; $\tau(\Delta\lambda)$ is characterized by 3 quantities; the maximum value τ_0 and the values τ_1 and τ_2 corresponding to the half widths $\Delta\lambda_1=0.3$ Å and $\Delta\lambda_2=0.53$ Å. The code fits S and $\Delta\lambda_D$ by the conditions:

$$\tau_1=\tau_0\exp(-(\Delta\lambda_1/\Delta\lambda_D)^2)$$

$$\tau_2=\tau_0\exp(-(\Delta\lambda_2/\Delta\lambda_D)^2) \quad (6)$$

coupled with Eq. (1). The code rejects values of radial velocities corresponding to $\Delta\lambda_1$ and $\Delta\lambda_2$ which are too different and also the $\delta\tau$-functions which are not increasing monotonically on the blue side between τ_1 and τ_0 or decreasing monotonically on the red side between τ_0 and τ_1. Figure 9 shows that there is a linear correlation between the velocity values obtained by these two methods. However, no obvious correlation between the values of the source function or the Doppler width calculated by these two different codes based on the cloud model was found. The differences are due to the fact that the "3-optical depths" method does not assume a gaussian profile for the optical depth and, because of the method of adjusting the source function, it may have multiple solutions in the case of large asymmetries.

The existence of a correlation of the velocity values suggests that out of the 4 parameters, the one most decoupled from the others is the velocity, a suggestion already made by Durrant

© European Southern Observatory • Provided by the NASA Astrophysics Data System

1990A&A...230..200A

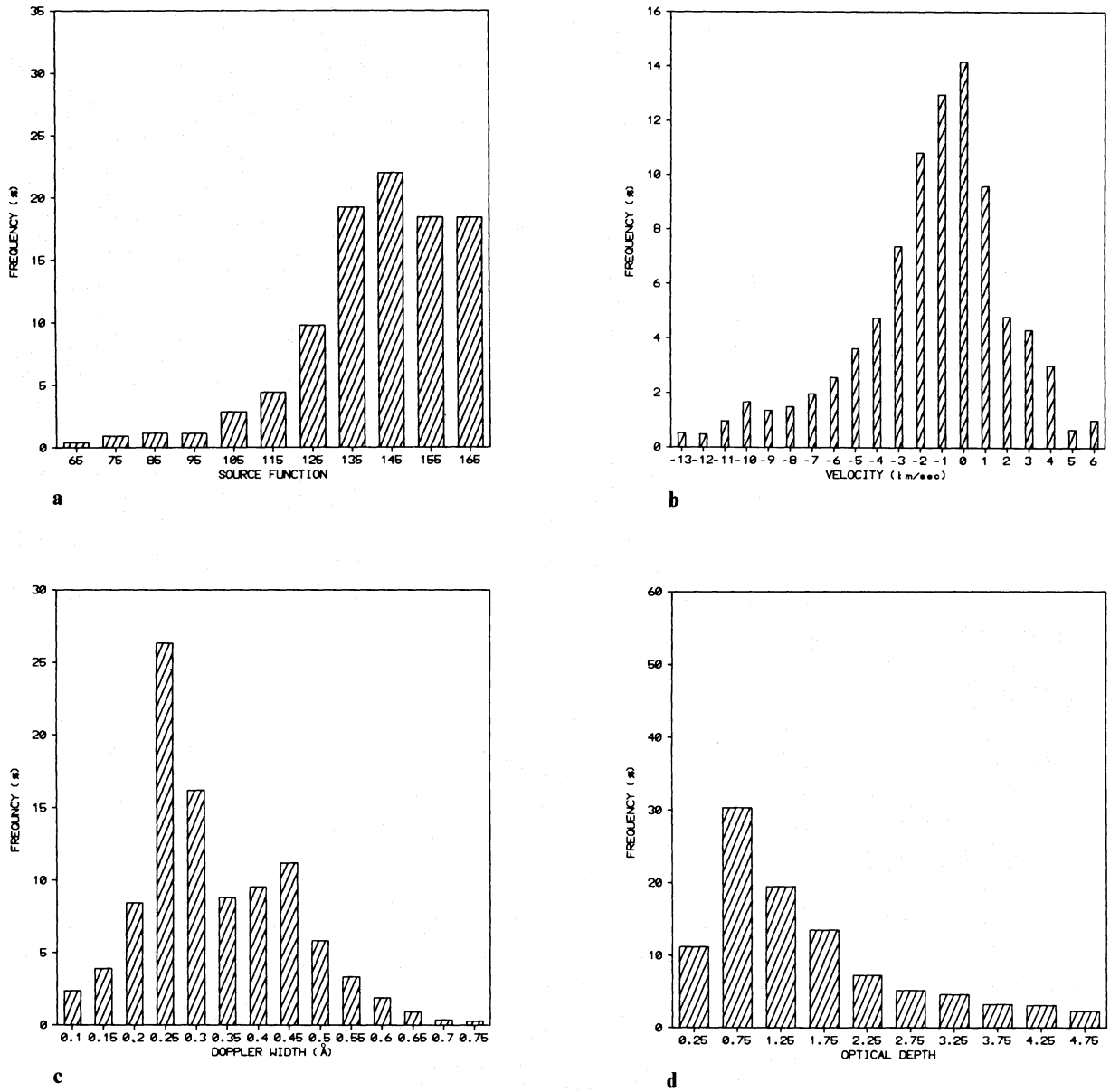

Fig. 6a–d. Histograms of the 4 parameters derived with the cloud model in the fibril region: **a** source function; **b** velocity; **c** Doppler width; **d** optical depth

(1975). In order to confirm this, another method proposed by Mein et al. (1985) for a fast calculation of the velocity was used. According to this method the source function is assumed to be given (e.g. $S/I_0 \sim 0.65$ or 0.95) and the velocity is computed from the position of the barycenter of the $\tau(\Delta\lambda)$ function. A scatter plot of the velocities calculated assuming these two different values of the source function shows also a linear correlation. Moreover a scatter plot between the velocities calculated with our cloud model method and the velocities calculated by this latter method shows a linear correlation too (Fig. 10).

Using the latter method (e.g. $S/I_0 = 0.95$) we have examined the influence on the velocity values, of two different background profiles corresponding to the quiet regions and the active regions of the observed field, respectively. In the latter case the velocities are too low, approaching the values given by the Doppler shift method (Fig. 11). Thus the selection of the appropriate background profile must be reexamined.

6. Summary and conclusions

The cloud model offers the attractive possibility of deriving several physical parameters of chromospheric features. However only under a restricted range of circumstances do these parameters reflect accurately the atmospheric properties. Absorbing features, lying above the average level of the chromosphere, are ideal for the application of the cloud model. For such features we have mapped the spatial variation of the source function, the line-of-sight velocity, the optical depth and Doppler width.

A comparison of the velocities determined with the cloud model with those derived with the Doppler shift method at

© European Southern Observatory • Provided by the NASA Astrophysics Data System

1990A&A...230..200A

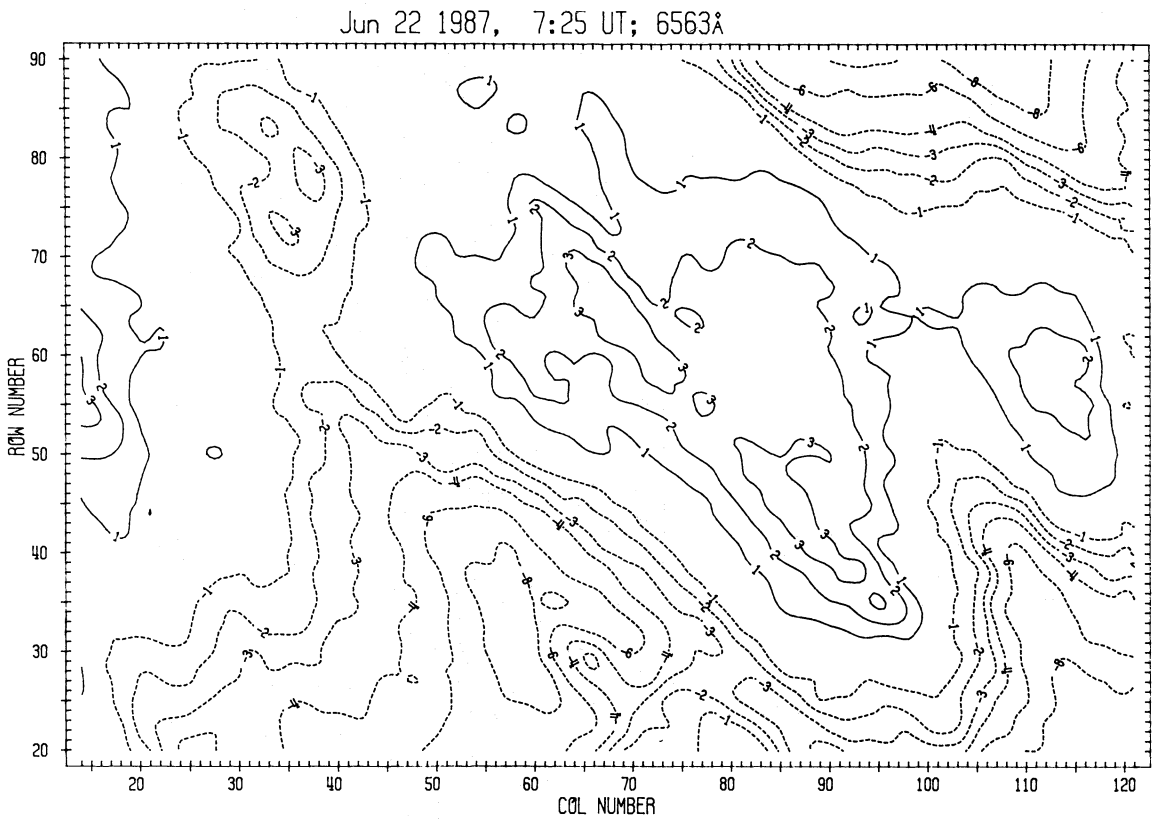

Fig. 7. Contour map of the velocity in the AFS region obtained with the Doppler shift method at ± 0.3 Å

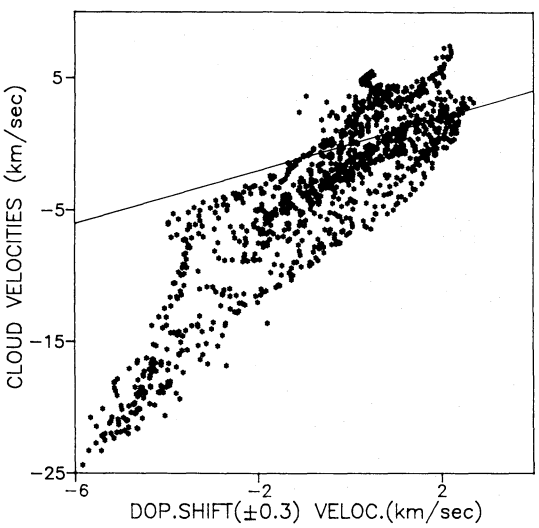

Fig. 8. Comparison of the velocities given by the cloud model and the Doppler shift method at ± 0.3 Å in the AFS region. The solid line corresponds to equal velocities

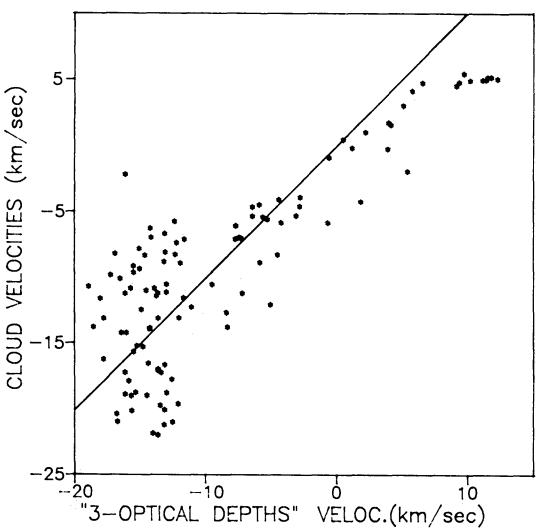

Fig. 9. Comparison of the velocities given by the cloud model and the "3-optical depths" method. The solid line corresponds to equal velocities

± 0.3 Å showed that the latter underestimates their value by more than a factor of 2. This is not surprising, considering the fact that the optical depth of the features at the line center is of the order of unity and their Doppler width is of the order of 0.5 Å. This implies that at ± 0.3 Å we have significant contribution from the unshifted background profile and hence the Doppler shift method gives lower velocity.

The cloud velocities are consistent with the results of the "3-optical depths" method of Mein and Mein (1988), although values at individual pixels are somewhat different. However, the two methods give different results for the other parameters, probably due to the different assumptions involved. The fact that, in spite of these differences, the two methods give consistent velocities shows that the velocity is not strongly coupled with the

© European Southern Observatory • Provided by the NASA Astrophysics Data System

1990A&A...230..200A

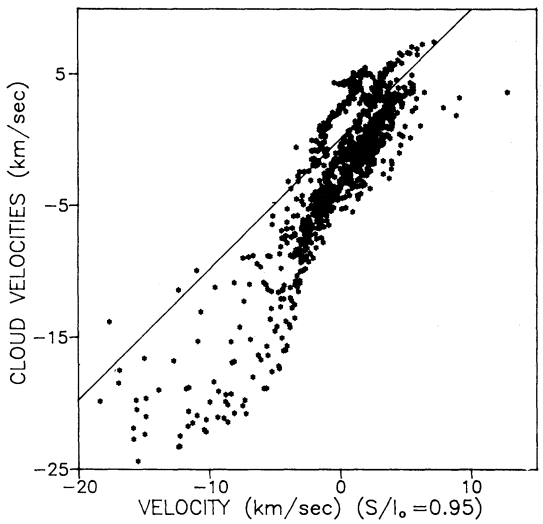

Fig. 10. Comparison of the velocities given by the cloud model and under the assumption of given source function, equal to I_0 0.95, in the AFS region. The solid line corresponds to equal velocities

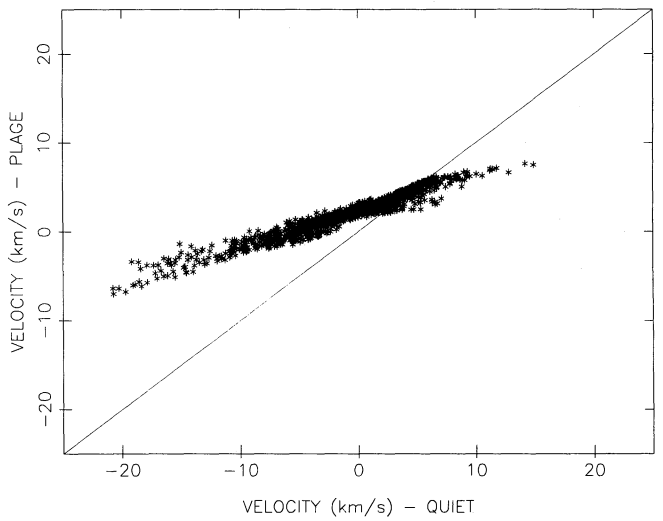

Fig. 11. Comparison of the velocities under the assumption of given source function (equal to I_0 0.95) for two different background profiles corresponding to the quiet and the active Sun. The solid line corresponds to equal velocities

other three parameters. This confirms the theoretical result of Durrant (1975) and it is further supported by our result that the computed velocity is relatively insensitive to the precise value of the source function.

Our velocity maps of an arch filament region show that only one filament out of three exhibits the classical type of motion, i.e. material ascending near the top and descending at the footpoints. The velocity map of a sunspot superpenumbra region shows motions which are overall consistent with the chromospheric Evershed flow. The superpenumbral fibrils have a smaller Doppler width than the AFS; if the two structures have comparable temperature, the microturbulent velocity is much higher in the latter.

Both in the arch filaments and the superpenumbral fibrils the source function increases towards the edge of the features, while the optical depth and the Doppler width show an anticorrelation, implying that the column density of the emitting material varies little over the structures; we estimate it to be about $5.2\,10^{12}$ cm^{-2} for the AFS and $3.7\,10^{12}$ cm^{-2} for the superpenumbral fibrils which give values for N_2 in the range $2\text{–}3\,10^4$ cm^{-3} and $0.7\text{–}1.3\,10^4$ cm^{-3} respectively.

Apart from this anticorrelation, no other dependence was found between any two of the cloud parameters. Thus the suggestion by several authors (Gebbie and Steinitz, 1974; Durrant, 1975; Steinitz et al., 1977) that the source function in a cloud is not a free parameter, but depends on the Doppler width is not verified in our set of data. This suggestion was based on the fact that under typical chromospheric conditions Hα is a photoionization controlled line.

We found no correlation between the wavelength of highest contrast and the line-of-sight velocity. This result clearly invalidates the idea that the velocity of an absorbing Hα feature can be estimated from the wavelength where the feature is most prominent.

This work demonstrated that the cloud model can be used efficiently in conjunction with the MSDP observations. It provides a powerful tool for the study of the spatial and temporal variations in a variety of solar features. Further work will include the study of temporal variations as well as the interpretation of the observed line-of-sight velocities.

Acknowledgements. The authors are indebted to J.M. Malherbe, B. Schmieder, C. Coutard, R. Hellier for MSDP observations and C. Brechet for data processing. Travel funds for this work were provided in part through the bilateral scientific exchange programs between France and Greece.

References

Alissandrakis, C.E., Dialetis, D., Mein, P., Schmieder, B., Simon, G.: 1988, *Astron. Astrophys.* **201**, 339
Athay, R.G.: 1970, *Solar Phys.* **12**, 175
Beckers, J.M.: 1964, Ph.D. Thesis, Utrecht
Beckers, J.M.: 1968, *Solar Phys.* **3**, 367
Bray, R.J.: 1973, *Solar Phys.* **29**, 317
Bray, R.J.: 1974, *Solar Phys.* **38**, 377
Bray, R.J., Loughhead, R.E.: 1983, *Solar Phys.* **85**, 131
Bruzek, A.: 1967, *Solar Phys.* **2**, 451
Bruzek, A.: 1969, *Solar Phys.* **8**, 29
Cram, L.E.: 1986, *Astrophys. J.* **300**, 830
Dialetis, D., Mein, P., Alissandrakis, C.E.: 1985, *Astron. Astrophys.* **147**, 93
Durrant, C.J.: 1975, *Solar Phys.* **44**, 41
Grosmann-Doerth, U., von Uexküll, M.: 1971, *Solar Phys.* **20**, 31
Grosmann-Doerth, U., von Uexküll, M.: 1973. *Solar Phys.* **28**, 319
Grosmann-Doerth, U., von Uexküll, M.: 1973, *Solar Phys.* **30**, 71
Grosmann-Doerth, U., von Uexküll, M.: 1977, *Solar Phys.* **55**, 321
Kulander, J.L., Jefferies, J.T.: 1966, *Astrophys. J.* **146**, 194
Loughhead, R.E.: 1973, *Solar Phys.* **29**, 327
Mein, P.: 1977, *Solar Phys.* **54**, 55
Mein, P., Mein, N., Malherbe, J.M.: 1985, MPA/LPARL Workshop in Munich, p. 303
Mein, P., Mein, N.: 1988, *Astron. Astrophys.* **203**, 162
Steinitz, R., Gebbie, K.B., Bar, V.: 1977, *Astrophys. J.* **213**, 269
Vernazza, J.E., Avrett, E.H., Loeser, R.: 1973, *Astrophys. J.* **184**, 605

© European Southern Observatory • Provided by the NASA Astrophysics Data System